Pairwise Three-Dimensional Shape Context for Partial Object Matching and Retrieval on Mobile Laser Scanning Data

Article *in* IEEE Geoscience and Remote Sensing Letters · May 2014

DOI: 10.1109/LGRS.2013.2285237

CITATIONS
10

READS
68

5 authors, including:

Yongtao Yu
Huaiyin Institute of Technology
41 PUBLICATIONS **370** CITATIONS
SEE PROFILE

Jonathan Li
University of Waterloo
254 PUBLICATIONS **3,243** CITATIONS
SEE PROFILE

Haiyan Guan
Nanjing University of Information Science & …
52 PUBLICATIONS **428** CITATIONS
SEE PROFILE

Cheng Wang
Xiamen University
157 PUBLICATIONS **894** CITATIONS
SEE PROFILE

Pairwise Three-Dimensional Shape Context for Partial Object Matching and Retrieval on Mobile Laser Scanning Data

Yongtao Yu, Jonathan Li, *Senior Member, IEEE*, Jun Yu, *Member, IEEE*, Haiyan Guan, and Cheng Wang, *Member, IEEE*

***Abstract*—A novel pairwise 3-D shape context for partial object matching and retrieval is developed for extracting 3-D light poles and trees from mobile laser scanning (MLS) point clouds in a typical urban street scene. Unlike the single-point shape context describing only the local topology of a shape, the pairwise 3-D shape context can simultaneously model the local and global geometric structures of a shape in manifold space. By using histogram descriptors, the pairwise 3-D shape context has such characteristics as invariance to scale, invariance to orientation, and partial insensitivity to topological changes. Our results show that 3-D light poles and individual trees can be extracted from the RIEGL VMX-450 MLS point clouds and the performance achieved using our algorithm is much more accurate and effective than those of the other two existing algorithms.**

***Index Terms*—Correspondence, mobile laser scanning (MLS), object matching, object retrieval, shape context.**

I. Introduction

TECHNOLOGIES on automated object extraction and detailed 3-D object reconstruction in urban environments are currently in demand in the fields of photogrammetry, remote sensing, and computer vision. Detailed geometric information of 3-D objects plays an important role in modeling and reconstructing real-world objects. Therefore, accurate and cost-effective extraction of objects from big data or complex environments has drawn many researchers' interest. Much work has been conducted on the exploration of shape descriptors to model the relative relationship of a point with its nearest neighbors [1]. However, because of the diversity of objects within the same category, the different environments of the same object, and the similarity between the objects from different categories, it is challenging to define a general model to describe the geometric structure of a shape from a specific class of objects.

In general, 3-D shapes are described by the following three main types of input data: 1) point sets; 2) oriented points; and 3) surfaces (or meshes). Based on the representations of shape descriptors, shape matching methods are divided into three broad categories [1]: 1) feature-based methods [2]–[4]; 2) graph-based methods [5]–[7]; and 3) geometry-based methods [8]–[11]. Heat kernel maps [12] and persist heat signatures [13] were developed for matching partial and incomplete shapes. Instead of using local single-point-based shape descriptors, pairwise shape descriptors [14], [15] were developed for shape matching and retrieval. However, these methods required that the input data must be meshes. Thus, it is challenging to directly transplant these methods to unoriented sparse 3-D point sets.

In the past decades, light detection and ranging (LiDAR) technologies have been rapidly developed for the acquisition of geospatial information. Due to the capability of the LiDAR systems in measuring the surface topography directly, the high-density high-accuracy 3-D point clouds acquired by the LiDAR systems have enriched the corpus of 3-D data and become a leading source for various applications. Algorithms for object detection and retrieval (e.g., trees [16], [17], roads [18], and buildings [19]) from LiDAR point clouds have also been presented in the literature.

In this letter, we propose a novel pairwise 3-D shape context for partial object matching and retrieval on mobile laser scanning (MLS) point clouds. Unlike the existing local point-based shape contexts which only model the local topology of a feature point, the pairwise 3-D shape context, which is an object-oriented shape context and defined in manifold space, can do the following: 1) describe the local topology of a specific point and 2) model the global geometric structure of a shape through pairwise combinations. By using histogram descriptors, the pairwise 3-D shape context has such characteristics as invariance to scale, invariance to orientation, and partial insensitivity to topological changes. The pairwise 3-D shape context has been tested in shape correspondence and object retrieval on the MLS point clouds acquired by a RIEGL VMX-450 MLS system. The results demonstrate the efficiency and feasibility of the proposed pairwise 3-D shape context in partial object matching and retrieval.

II. Pairwise 3-D Shape Context

The pairwise 3-D shape context of a point is depicted by histogram descriptors in manifold space. The histogram

Manuscript received September 18, 2013; accepted October 2, 2013. Date of publication October 25, 2013; date of current version December 11, 2013.

Y. Yu, J. Yu, and C. Wang are with the Key Laboratory of Underwater Acoustic Communication and Marine Information Technology (Ministry of Education), School of Information Science and Engineering, Xiamen University, Xiamen 361005, China.

J. Li is with the Key Laboratory of Underwater Acoustic Communication and Marine Information Technology (Ministry of Education), School of Information Science and Engineering, Xiamen University, Xiamen 361005, China, and also with the GeoSpatial Technology and Remote Sensing Laboratory, Faculty of Environment, University of Waterloo, Waterloo, ON N2L 3G1, Canada (e-mail: junli@xmu.edu.cn).

H. Guan is with the GeoSpatial Technology and Remote Sensing Laboratory, Faculty of Environment, University of Waterloo, Waterloo, ON N2L 3G1, Canada.

Color versions of one or more of the figures in this paper are available online at http://ieeexplore.ieee.org.

Digital Object Identifier 10.1109/LGRS.2013.2285237

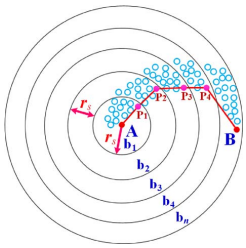

Fig. 1. Model of computing the shortest radial path.

descriptor is constructed automatically as follows: 1) Determine the region of interest (ROI) between a pair of points; 2) partition the ROI into bin structures with either equal intervals or log-polar intervals along the radial direction; and 3) analyze and normalize the point distributions within each bin.

A. Construction of the ROI

In this section, we present a detailed construction of the ROI. Given a pair of 3-D points (A, B), we first find the shortest path from A to B in manifold space, followed by determining the point region that models the geometric structure between A and B.

Shortest Radial Path: We define a new method to compute the shortest radial path that well describes the topology between two points in manifold space. As shown in Fig. 1, the shortest radial path from A to B is defined as $P_{AB} = [p_0, p_1, \ldots, p_{n-1}, p_n]$, where $A = p_0$ and $B = p_n$. First, we construct a set of concentric spheres $(b_1, b_2, \ldots, b_n)$ with equal radial intervals (r_s) centered at point A. Here, $p_1 \in b_1$, $p_2 \in b_2 \setminus b_1, \ldots, p_n \in b_n \setminus b_{n-1}$. Next, we recursively construct the shortest radial path from A to B as follows: 1) Determine p_{n-1} as the nearest point to B in $b_{n-1} \setminus b_{n-2}$, i.e., $p_{n-1} = \arg\min_{p \in b_{n-1} \setminus b_{n-2}} \|p - B\|_2$, and denote the direct path from p_{n-1} to B as $R_{p_{n-1}B}$; 2) compute the shortest radial path from A to p_{n-1} $(P_{Ap_{n-1}})$; and 3) concatenate $P_{Ap_{n-1}}$ and $R_{p_{n-1}B}$ to construct the shortest radial path from A to B. The aforementioned three criteria are expressed as follows:

$$P_{AB} = \begin{cases} R_{AB}, & B \in b_1 \\ P_{Ap_{n-1}} + R_{p_{n-1}B}, & B \in b_n \setminus b_{n-1} \wedge p_{n-1} \in b_{n-1} \setminus b_{n-2}. \end{cases} \tag{1}$$

ROI: After computing the shortest radial path from A to B, we then construct the ROI for the pair of points (A, B), within which the distribution of points models the geometric structure of a specific shape. First, as shown in Fig. 2(a), we create a scalar field as the initial region, which is given by the points whose distances to the shortest radial path P_{AB} lie below a threshold r_p. The parameter r_p is the relative width of the initial region. In practice, instead of selecting a specific value for r_p, we select the width relative to the distance along the shortest radial path and define the width-to-distance ratio (θ_p) as follows:

$$\theta_p = \frac{r_p}{d_{AB}} \tag{2}$$

where d_{AB} is the length of the shortest radial path P_{AB}. Next, we create a filtering region for pruning the initial region. As shown in Fig. 2(b), the filtering region is defined as the intersection of the spherical region centered at point A and the spherical region centered at point B. Finally, as shown in Fig. 2(c), we construct the ROI by intersecting the initial region and the filtering region.

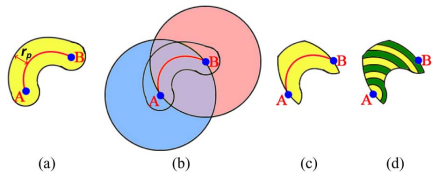

Fig. 2. ROI construction and bin partition models: (a) Initial region, (b) filtering region, (c) final ROI, and (d) bin partition model with equal intervals.

B. Construction of Histogram Descriptor

Bin Partition Model: After constructing the ROI, we partition it into a set of bins describing the local statistical distribution between points A and B. There are two strategies for partitioning the ROI: 1) Partition the ROI with equal radial intervals along the shortest radial path, and 2) partition the ROI with log-polar intervals along the shortest radial path. Fig. 2(d) shows a bin partition model with equal radial intervals from A to B. The interval, denoted by r_b, is determined as follows:

$$r_b = \frac{L_{AB}}{K_b} \tag{3}$$

where L_{AB} is the Euclidean distance between A and B and K_b is the bin number. In terms of the log-polar interval, the radius of the ith bin is defined as

$$r_{b_i} = \frac{L_{AB}}{K_b} \log_2 \left(2^{K_b} \frac{i}{K_b} \right), \qquad i = 1, 2, \ldots, K_b. \tag{4}$$

Histogram Descriptor: We use histogram descriptors to define the pairwise 3-D shape context. For a pair of points (A, B), the corresponding histogram descriptor h_{AB}, whose entries correspond to the bins of the ROI, is defined as

$$h_{AB}(k) = \frac{\#\{p \in \text{bin}(k)\}}{\sum_{i=1}^{K_b} \#\{q \in \text{bin}(i)\}}, \qquad k = 1, 2, \ldots, K_b. \tag{5}$$

Our construction produces a directional histogram descriptor, i.e., the histogram descriptor h_{AB} of the pair of points (A, B) is different from the histogram descriptor h_{BA} of the pair of points (B, A).

C. Properties of the Pairwise 3-D Shape Context

Invariance to Scale: Given a pair of points (A, B) on an object, the ROI between A and B is constructed based on the shortest radial path P_{AB} and the width ratio θ_p. When the object is transformed by a scale of δ, the new histogram descriptor h'_{AB} becomes

$$\begin{aligned} h'_{AB}(k) &= \frac{\#\{p \in \text{bin}(k)\} \cdot \delta^2}{\sum_{i=1}^{K_b} \#\{q \in \text{bin}(i)\} \cdot \delta^2} = \frac{\#\{p \in \text{bin}(k)\}}{\sum_{i=1}^{K_b} \#\{q \in \text{bin}(i)\}} \\ &= h_{AB}(k), \qquad k = 1, 2, \ldots, K_b. \end{aligned} \tag{6}$$

Thus, the pairwise 3-D shape context is invariant under scaling.

Invariance to Orientation: Given a pair of points (A, B) on an object, translating or rotating the object does not affect the construction of the ROI between the points because all

measurements are taken with respect to the relative relationship between A and B. Thus, the pairwise 3-D shape context is invariant under translating and rotating.

Partial Insensitivity to Topological Changes: Since our construction is based on the shortest radial path between two points, the pairwise 3-D shape context is affected only when the shortest radial path is unstable. However, the paradigm of using pairs of points makes this approach partially insensitive to topological changes. When a local topological change occurs, most of the histogram descriptors still remain intact because the local topological change affects only the descriptors related to points in their vicinities.

III. Results and Discussion

The point cloud data used in our experiments were acquired by a RIEGL VMX-450 MLS system on Xiamen Island, China. This system consists of two full-view RIEGL VQ-450 laser scanners, an Inertial Measurement Unit/Global Navigation Satellite System, a wheel-mounted Distance Measurement Indicator, and four high-resolution cameras. The accuracy of the scanned point clouds is within 8 mm (1σ standard deviation), and the precision is 5 mm.

A. Shape Correspondence

A variety of methods that use local shape descriptors for correspondence have been proposed in the literature [20]. In this section, we test the proposed pairwise 3-D shape context for correspondence on the MLS point clouds. Given two objects P and Q, we first sampled a set of points from each of these two objects, respectively. In our experiments, we used the sampling method mentioned in [21] to sample N (e.g., $N = 20$) points from each object. For a sample point p, its shape context with respect to pairwise combinations with the remaining sample points is defined as

$$\boldsymbol{H}_p = \left[h_1^p, h_2^p, \ldots, h_{N-1}^p\right] \in R^{K_b \times (N-1)} \tag{7}$$

where h_i^p $(i = 1, 2, \ldots, N-1)$ denotes the histogram descriptor defined in (5).

Consider a point p on object P and a point q on object Q. Since the shape contexts are distributions represented as histograms, the cost of matching these two points is naturally defined using χ^2 distance as follows:

$$C(p,q) = \min_{i,j=1}^{N-1} \frac{1}{2} \sum_{k=1}^{K_b} \frac{\left[h_i^p(k) - h_j^q(k)\right]^2}{h_i^p(k) + h_j^q(k)}. \tag{8}$$

Then, the cost matrix $C \in R^{N \times N}$, whose entry $C(i,j)$ denotes the cost of matching points i and j, for matching objects P and Q is constructed. Finally, the one-to-one matching between the points on object P and the points on object Q is given by

$$M(\pi) = \min_{\pi} \frac{1}{N} \sum_{i=1}^{N} C\left(i, \pi(i)\right) \tag{9}$$

where π is a permutation of $\{1, 2, \ldots, N\}$. This is an instance of the square assignment (or weighted bipartite matching) problem, which can be solved in $O(N^3)$ time using the Hungarian method [22]. In our experiments, we used the more efficient algorithm proposed in [23].

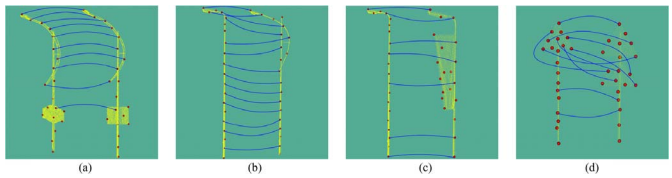

Fig. 3. Correspondences computed with the pairwise 3-D shape context.

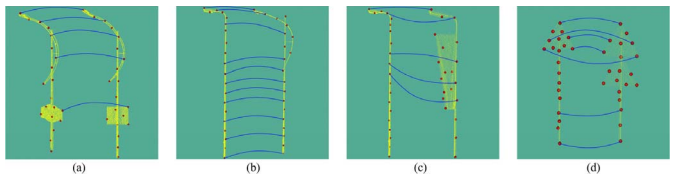

Fig. 4. Correspondences computed with the single-point 3-D shape context.

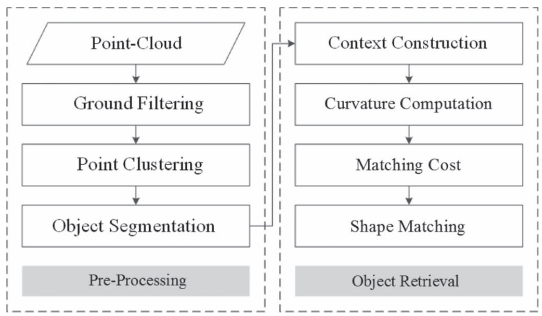

Fig. 5. Flowchart of the object retrieval method.

Results With the Pairwise 3-D Shape Context: In Fig. 3, we present visual examples of correspondences computed using the pairwise 3-D shape context with $r_s = 0.3$ m, $\theta_p = 0.2$, and $K_b = 30$. The pairwise 3-D shape context can provide meaningful and correct matches for objects with missing parts, or even different topologies. Thus, the proposed pairwise 3-D shape context is suitable for partial object matching.

Comparison With the Single-Point 3-D Shape Context: To compare the proposed pairwise 3-D shape context with other local shape descriptors, we conducted several experiments using the single-point 3-D shape context [24] to compute correspondences (Fig. 4). By comparing the correspondences in Fig. 4 with those in Fig. 3, we conclude that the proposed pairwise 3-D shape context performs better than the single-point 3-D shape context in partial object matching.

B. Object Retrieval

Fig. 5 shows the flowchart of the proposed object retrieval method. The point clouds are first preprocessed by filtering out the ground points and segmenting the off-ground points into clustered objects [25]. N (e.g., $N = 20$) points are then sampled from each object. After the pairwise 3-D shape context is constructed with $r_s = 0.3$ m, $\theta_p = 0.2$, and $K_b = 30$, the curvature for each sample point p is computed by

$$\sigma_p = \frac{\lambda_0}{\lambda_0 + \lambda_1 + \lambda_2} \tag{10}$$

where λ_0, λ_1, and λ_2 $(\lambda_0 \leq \lambda_1 \leq \lambda_2)$ are the eigenvalues obtained by decomposing the covariance matrix of point p. The

TABLE I
LIGHT POLE RETRIEVAL RESULTS FOR LIGHT POLE DATA SETS

	Ground-truth of light poles				Light pole retrieval results			
	Size (GB)	Clean	Attachment	Total	Clean	Attachment	Total	Rate (%)
Dataset-1	3.79	40	40	80	40	39	79	98.75
Dataset-2	7.64	38	59	97	38	55	93	95.88
Dataset-3	8.55	59	57	116	59	55	114	98.28

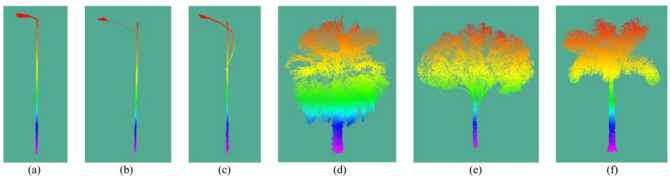

Fig. 6. Illustration of prototypes for six different data sets.

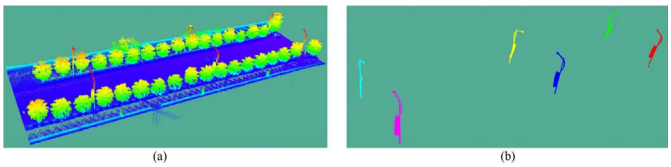

Fig. 7. Part of Dataset-3: (a) Raw point cloud and (b) extracted light poles.

covariance matrix of point p is constructed using the k nearest neighbors $(p_1, p_2, \ldots, p_k)$ of p as follows:

$$C_p = \frac{1}{k+1}\sum_{i=0}^{k}(p_i - \overline{p}) \cdot (p_i - \overline{p})^{\mathrm{T}} \tag{11}$$

where $p_0 = p$ and $\overline{p} = (1/(k+1))\sum_{i=0}^{k} p_i$ is the centroid of the $k+1$ points. The objective function for measuring the similarity and matching between objects P and Q is defined as

$$O(P,Q) = \min_{\pi} \frac{1}{N}\sum_{i=1}^{N} C\left(i, \pi(i)\right) + \frac{1}{N}\sum_{i=1}^{N} |\sigma_{p_i} - \sigma_{q_i}| + \frac{1}{N(N-1)}\sum_{i=1}^{N}\sum_{j=1}^{N-1} \min_{m,n} \left\| H_{p_i}(j) - H_{q_m}(n) \right\|_1 . \tag{12}$$

The first part in (12) corresponds to (9), the second part serves to measure the local similarity between two objects, and the last part aims to measure the global similarity between two objects.

Table I shows the light pole retrieval results obtained from the three selected data sets with different light pole types, shown in Fig. 6(a)–(c). In Table I, "Size" denotes the size of the data set in gigabytes, "Clean" denotes the number of light poles without any attachments (e.g., traffic signs and advertising boards), "Attachment" denotes the number of light poles with attachments, "Total" denotes the total number of light poles, and "Rate" denotes the light pole retrieval rate. Fig. 7 presents a part of the raw point cloud from Dataset-3 along with the extracted light poles. Table II presents the tree retrieval results for the three selected data sets with different tree types, shown in Fig. 6(d)–(f). Fig. 8 shows a part of the raw point cloud from Dataset-6 along with the extracted trees. Based on these results, we can conclude that the proposed pairwise 3-D shape context is able to model and distinguish the geometric structure of a shape, even when partial missing or partial topological change exists, and to achieve a good performance in 3-D object retrieval.

TABLE II
TREE RETRIEVAL RESULTS FOR TREE DATA SETS

	Ground-truth of trees		Tree retrieval results	
	Size (GB)	Number of trees	Number of trees	Rate (%)
Dataset-4	3.27	205	202	98.54
Dataset-5	2.09	119	118	99.16
Dataset-6	6.52	346	339	97.98

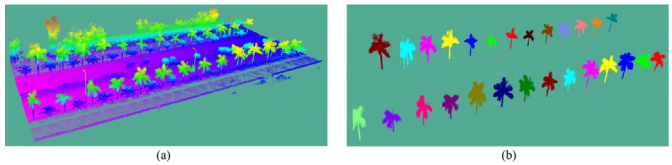

Fig. 8. Part of Dataset-6: (a) Raw point cloud and (b) extracted trees.

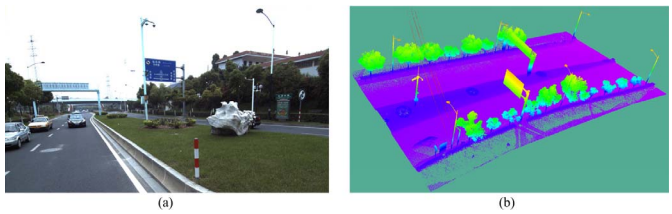

Fig. 9. (a) Photograph of the study area and (b) the point cloud coverage.

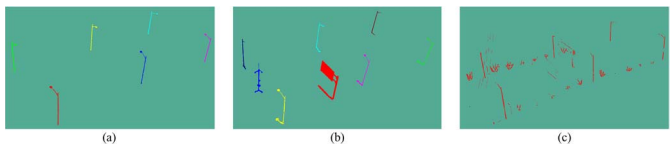

Fig. 10. Retrieval results of light poles using (a) our proposed algorithm, (b) the DoPP algorithm, and (c) the PCA-based algorithm.

C. Comparative Study

To further demonstrate the efficiency and correctness of the proposed algorithm in 3-D object retrieval, a study was carried out to compare the performance of our proposed algorithm with those of the Density of Projected Points (DoPP) algorithm [26] and the Principal Component Analysis (PCA) based algorithm [27] on light pole retrieval. Fig. 9 presents a photograph of the study area along with the point cloud coverage of this area. Fig. 10 shows the better retrieval results of the light poles using our proposed algorithm [Fig. 10(a)] over the other two existing algorithms [Fig. 10(b) and (c)].

IV. CONCLUSION

This letter has presented a novel pairwise 3-D shape context for modeling the geometric structure of a shape in a typical urban street scene. The results obtained from six MLS data sets demonstrate that the pairwise 3-D shape context has the capabilities to describe the local topology of a point and to model the global geometric structure of a shape. By using histogram descriptors, the pairwise 3-D shape context has the

properties of invariance to scale, invariance to orientation, and partial insensitivity to topological changes. The results also show that the pairwise 3-D shape context can match more homologous points and achieve better performance in 3-D object retrieval. A comparative study demonstrates that our proposed algorithm achieved the highest correctness and efficiency over the other two existing algorithms. However, due to the pairwise scheme, the construction of the pairwise 3-D shape context is slower than that of the single-point-based 3-D shape context. In practice, parallel computing and multithread techniques may be used to speed up processing and further improve the efficiency of 3-D object retrieval from big point cloud data.

ACKNOWLEDGMENT

The authors would like to thank M. McAllister, a Sessional Lecturer in English at Xiamen University, for his assistance in proofreading this letter.

REFERENCES

[1] J. W. H. Tangelder and R. C. Veltkamp, "A survey of content based 3D shape retrieval methods," *Multimedia Tools Appl.*, vol. 39, no. 3, pp. 441–471, Sep. 2008.

[2] J. Corney, H. Rea, D. Clark, J. Pritchard, M. Breaks, and R. Macleod, "Coarse filters for shape matching," *IEEE Comput. Graph. Appl.*, vol. 22, no. 3, pp. 65–74, May 2002.

[3] R. Osada, T. Funkhouser, and B. Chazelle, "Shape distributions," *ACM Trans. Graph.*, vol. 24, no. 4, pp. 807–832, Oct. 2002.

[4] I. Kolonias, D. Tzovaras, S. Malassiotis, and M. G. Strintzis, "Fast content-based search of VRML models based on shape descriptors," *IEEE Trans. Multimedia*, vol. 7, no. 1, pp. 114–126, Feb. 2005.

[5] E. Zuckerberger, A. Tal, and S. Shlafman, "Polyhedral surface decomposition with applications," *Comput. Graph.*, vol. 26, no. 5, pp. 733–743, Oct. 2002.

[6] H. Sundar, D. Silver, N. Gagvani, and S. Dickinson, "Skeleton based shape matching and retrieval," in *Proc. Shape Modeling Int.*, Seoul, Korea, 2003, pp. 130–142.

[7] M. Hilaga, Y. Shinagawa, T. Kohmura, and T. L. Kunii, "Topology matching for fully automatic similarity estimation of 3D shapes," in *Proc. SIGGRAPH*, New York, NY, USA, 2001, pp. 203–212.

[8] T. Funkhouser, P. Min, M. Kazhdan, J. Chen, A. Halderman, D. Dobkin, and D. Jacobs, "A search engine for 3D models," *ACM Trans. Graph.*, vol. 22, no. 1, pp. 83–105, Jan. 2003.

[9] D. Zhang and G. Lu, "Shape-based image retrieval using generic Fourier descriptor," *Signal Process. Image Commun.*, vol. 17, no. 10, pp. 825–848, Nov. 2002.

[10] J. W. H. Tangelder and R. C. Veltkamp, "Polyhedral model retrieval using weighted point sets," *Int. J. Image Graph.*, vol. 3, no. 1, pp. 209–229, Jan. 2003.

[11] T. Funkhouser, M. Kazhdan, P. Shilane, P. Min, W. Kiefer, A. Tal, S. Rusinkiewicz, and D. Dobkin, "Modeling by example," *ACM Trans. Graph.*, vol. 23, no. 3, pp. 652–663, Aug. 2004.

[12] M. Ovsjanikov, Q. Mérigot, F. Mémoli, and L. Guibas, "One point isometric matching with the heat kernel," *Comput. Graph. Forum*, vol. 29, no. 5, pp. 1555–1564, Jul. 2010.

[13] T. K. Dey, K. Li, C. Luo, P. Ranjan, I. Safa, and Y. Wang, "Persistent heat signature for pose-oblivious matching of incomplete models," *Comput. Graph. Forum*, vol. 29, no. 5, pp. 1545–1554, Jul. 2010.

[14] Y. Zheng, C. L. Tai, E. Zhang, and P. Xu, "Pairwise harmonics for shape analysis," *IEEE Trans. Vis. Comput. Graph.*, vol. 19, no. 7, pp. 1172–1184, Jul. 2013.

[15] O. V. Kaick, H. Zhang, and G. Hamarneh, "Bilateral maps for partial matching," *Comput. Graph. Forum*, pp. 189–200, Sep. 2013.

[16] J. Secord and A. Zakhor, "Tree detection in urban regions using aerial LiDAR and image data," *IEEE Geosci. Remote Sens. Lett.*, vol. 4, no. 2, pp. 196–200, Apr. 2007.

[17] W. Yao and Y. Wei, "Detection of 3-D individual trees in urban areas by combining airborne LiDAR and imagery," *IEEE Geosci. Remote Sens. Lett.*, vol. 10, no. 6, pp. 1355–1359, Nov. 2013.

[18] Y. W. Choi, Y. W. Jang, H. J. Lee, and G. S. Cho, "Three-dimensional LiDAR data classifying to extract road point in urban area," *IEEE Geosci. Remote Sens. Lett.*, vol. 5, no. 4, pp. 725–729, Oct. 2008.

[19] B. Yang, W. Xu, and Z. Dong, "Automated extraction of building outlines from airborne laser scanning point clouds," *IEEE Geosci. Remote Sens. Lett.*, vol. 10, no. 6, pp. 1399–1403, Nov. 2013.

[20] O. V. Kaick, H. Zhang, G. Hamarneh, and D. Cohen-Or, "A survey on shape correspondence," *Comput. Graph. Forum*, vol. 30, no. 6, pp. 1681–1707, Sep. 2011.

[21] D. P. Mitchell, "Spectrally optimal sampling for distribution ray tracing," *ACM SIGGRAPH Comput. Graph.*, vol. 25, no. 4, pp. 157–164, Jul. 1991.

[22] C. H. Papadimitriou and K. Stieglitz, *Combinatorial Optimization: Algorithms and Complexity*. Englewood Cliffs, NJ: Prentice-Hall, 1982.

[23] R. Jonker and A. Volgenant, "A shortest augmenting path algorithm for dense and sparse linear assignment problems," *Computing*, vol. 38, no. 4, pp. 325–340, 1987.

[24] M. Körtgen, G. J. Park, M. Novotni, and R. Klein, "3D shape matching with 3D shape contexts," in *Proc. 7th Central Eur. Semin. Comput. Graph.*, Budmerice, Slovakia, 2003, pp. 5–17.

[25] W. Yao, P. Krzystek, and M. Heurich, "Tree species classification and estimation of stem volume and DBH based on single tree extraction by exploiting airborne full-waveform LiDAR data," *Remote Sens. Environ.*, vol. 123, pp. 368–380, Aug. 2012.

[26] Y. Hu, X. Li, J. Xie, and L. Guo, "A novel approach to extracting street lamps from vehicle-borne laser data," in *Proc. IEEE Conf. Geoinform.*, Shanghai, China, 2011, pp. 1–6.

[27] S. I. El-Halawany and D. D. Lichti, "Detection of road poles from mobile terrestrial laser scanner point cloud," in *Proc. 2011 Int. Workshop M2RSM*, Xiamen, China, 2011, pp. 1–6.